

1 A Non-homogeneous Time Mixed Integer LP

2 Formulation for Traffic Signal Control

3 Iain Guilliard
4 National ICT Australia
5 7 London Circuit
6 Canberra, ACT, Australia
7 iguilliard@nicta.com.au

8 Scott Sanner
9 Oregon State University
10 1148 Kelley Engineering Center
11 Corvallis, OR 97331
12 scott.sanner@oregonstate.edu

13 Felipe W. Trevizan
14 National ICT Australia
15 7 London Circuit
16 Canberra, ACT, Australia
17 felipe.trevizan@nicta.com.au

18 Brian C. Williams
19 Massachusetts Institute of Technology
20 77 Massachusetts Avenue
21 Cambridge, MA 02139
22 williams@csail.mit.edu

23 4873 words + 8 figures + 0 table + 24 citations
24 (Weighted total words: 6873 out of 7000 + 35 references)
25 August 1, 2015

1 **ABSTRACT**

2 As urban traffic congestion is on the increase worldwide, it is critical to maximize capacity and
3 throughput of existing road infrastructure through optimized traffic signal control. To this end, we
4 build on the body of work in mixed integer linear programming (MILP) approaches that attempt to
5 jointly optimize traffic signal control over an entire traffic network and specifically on improving
6 the scalability of these methods for large numbers of intersections. Our primary insight in this
7 work stems from the fact that MILP-based approaches to traffic control used in a receding horizon
8 control manner (that replan at fixed time intervals) need to compute high fidelity control poli-
9 cies only for the early stages of the signal plan; therefore, coarser time steps can be employed to
10 “see” over a long horizon to preemptively adapt to distant platoons and other predicted long-term
11 changes in traffic flows. To this end, we contribute the queue transmission model (QTM) which
12 blends elements of cell-based and link-based modeling approaches to enable a non-homogeneous
13 time MILP formulation of traffic signal control. We then experiment with this novel QTM-based
14 MILP control in a range of traffic networks and demonstrate that the non-homogeneous MILP for-
15 mulation achieves (i) substantially lower delay solutions, (ii) improved per-car delay distributions,
16 and (iii) more optimal travel times over a longer horizon in comparison to the homogeneous MILP
1 formulation with the same number of binary and continuous variables.

2 INTRODUCTION

As urban traffic congestion is on the increase worldwide with estimated productivity losses in the hundreds of billions of dollars in the U.S. alone and immeasurable environmental impact (1), it is critical to maximize capacity and throughput of existing road infrastructure through optimized traffic signal control. Unfortunately, many large cities still use some degree of *fixed-time* control (2) even if they also use *actuated* or *adaptive* control methods such as SCATS (3) or SCOOT (4). However, there is further opportunity to improve traffic signal control even beyond adaptive methods through the use of *optimized* controllers as evidenced in a variety of approaches ranging from mixed integer (linear) programming (5, 6, 7, 8, 9, 10) to heuristic search (11, 12) to scheduling (13) to reinforcement learning (2). Such optimized controllers hold the promise of maximizing existing infrastructure capacity by finding more complex (and potentially closer to optimal) jointly coordinated intersection policies in comparison to heuristically-adaptive policies such as SCATS and SCOOT. However, optimized methods are computationally demanding and often do not guarantee *jointly* optimal solutions over a large intersection network either because (a) they only consider coordination of neighboring intersections or arterial routes or (b) they fail to scale to large intersection networks simply for computational reasons. We remark that the latter scalability issue is endemic to many mixed integer programming approaches to optimized signal control.

In this work, we build on the body of work in mixed integer linear programming (MILP) approaches that attempt to jointly optimize traffic signal control over an *entire traffic network* (rather than focus on arterial routes) and specifically on improving the scalability of these methods for large urban traffic networks. In our investigation of existing approaches in this vein, namely exemplar methods in the spirit of (7, 9, 10) that use a (modified) cell transmission model (CTM) (14, 15) for their underlying prediction of traffic flows, we remark that a major drawback is the CTM-imposed requirement to choose a predetermined *homogeneous* (and often necessarily small) time step for reasonable modeling fidelity. This need to model a large number of CTM cells with a small time step leads to MILPs that are exceedingly large and often intractable to solve.

Our primary insight in this work stems from the fact that MILP-based approaches to traffic control used in a receding horizon control manner (that replan at fixed time intervals) need to compute high fidelity control policies only for the early stages of the signal plan; therefore, coarser time steps can be employed to “see” over a long horizon to preemptively adapt to distant platoons and other predicted long-term changes in traffic flows. This need for non-homogeneous control in turn spawns the need for an additional innovation: we require a traffic flow model that permits non-homogeneous time steps and properly models the travel time delay between lights. To this end, we might consider CTM extensions such as the variable cell length CTM (16), stochastic CTM (17, 18), CTM extensions for better modeling freeway-urban interactions (19) including CTM hybrids with link-based models (20), asymmetric CTMs for better handling flow imbalances in merging roads (21), the situational CTM for better modeling of boundary conditions (22), and the lagged CTM for improved modeling of the flow density relation (23). However, despite the widespread varieties of the CTM and usage for a range of applications (24), there seems to be no extension that permits *non-homogeneous* time steps as proposed in our novel MILP-based control approach.

For this reason, as a major contribution of this work to enable our non-homogeneous time MILP-based model of joint intersection control, we contribute the queue transmission model (QTM) that blends elements of cell-based and link-based modeling approaches as illustrated and summarized in Figure 1. The QTM offers the following key benefits:

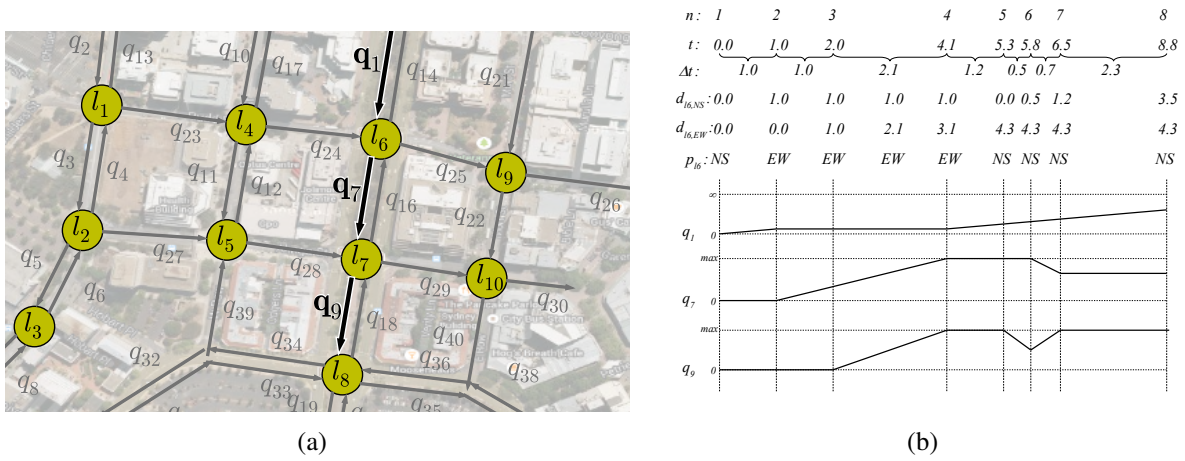


FIGURE 1 (a) Example of a real traffic network modeled using the QTM. (b) A preview of different QTM model parameters as a function of *non-homogeneous* discretized time intervals indexed by n . For each n , we show the following parameters: the elapsed time t , the non-homogeneous time step length Δt , the cumulative duration d of two different light phases for l_6 , the phase p of light l_6 , and the traffic volume of different queues q linearly interpolated between time points. There is technically a binary p for each phase, but we abuse notation and simply show the current active phase: *NS* for *north-south green* and *EW* for *east-west green* assuming the top of the map is north. Here we see that traffic progresses from q_1 to q_7 to q_9 according to light phases and traffic propagation delay with non-homogeneous time steps only at required changepoints. We refer to the QTM model section for precise notation and technical definitions.

- Unlike previous CTM-based joint intersection signal optimization (7, 9, 10), the QTM is intended for *non-homogeneous* time steps that can be used for control over large horizons.
- Any length of roadway without merges or diverges can be modeled as a single queue leading to compact QTM MILP encodings of large traffic networks (i.e., large numbers of cells and their associated MILP variables are not required *between* intersections).
- The QTM accurately models fixed travel time delays critical to green wave coordination as in (5, 6, 8) through the use of a non-first order Markovian update model and further combines this with fully joint intersection signal optimization in the spirit of (7, 9, 10).

In the remainder of this paper, we first formalize our novel QTM model of traffic flow with non-homogeneous time steps and show how to encode it as a linear program for computing traffic flows. Next we proceed to allow the traffic signals to become discrete phase variables that are optimized subject to a delay minimizing objective and standard minimum and maximum time constraints for cycles and phases; this results in our final MILP formulation of traffic signal control. We then experiment with this novel QTM-based MILP control in a range of traffic networks and demonstrate that the non-homogeneous MILP formulation achieves (i) substantially lower delay solutions, (ii) improved per-car delay distributions, and (iii) more optimal travel times over a longer horizon in comparison to the homogeneous MILP formulation with the same number of binary and continuous variables.

2 THE QUEUE TRANSMISSION MODEL (QTM)

3 A Queue Transmission Model (QTM) is the tuple $(\mathcal{Q}, \mathcal{L}, \vec{\Delta t}, \mathbf{I})$, where \mathcal{Q} and \mathcal{L} are, respectively,
 4 the set of queues and lights; $\vec{\Delta t}$ is a vector of size N representing the discretization of the problem
 5 horizon $[0, T]$ and the duration in seconds of the n -th time interval is denoted as Δt_n ; and \mathbf{I} is a
 6 matrix $|\mathcal{Q}| \times T$ in which $I_{i,n}$ represents the flow of cars requesting to enter queue i from the outside
 7 of the network at time n .

8 A **traffic light** $\ell \in \mathcal{L}$ is defined as the tuple $(\Psi_\ell^{\min}, \Psi_\ell^{\max}, \mathcal{P}_\ell, \vec{\Phi}_\ell^{\min}, \vec{\Phi}_\ell^{\max})$, where:

- 9 • \mathcal{P}_ℓ is the set of phases of ℓ ;
- 10 • Ψ_ℓ^{\min} (Ψ_ℓ^{\max}) is the minimum (maximum) allowed cycle time for ℓ ; and
- 11 • $\vec{\Phi}_\ell^{\min}$ ($\vec{\Phi}_\ell^{\max}$) is a vector of size $|\mathcal{P}_\ell|$ and $\Phi_{\ell,k}^{\min}$ ($\Phi_{\ell,k}^{\max}$) is the minimum (maximum) allowed
 12 time for phase $k \in \mathcal{P}_\ell$.

13 A **queue** $i \in \mathcal{Q}$ represents a segment of road that vehicles traverse at free flow speed; once
 14 traversed, the vehicles are vertically stacked in a stop line queue. Formally, a queue i is defined by
 15 the tuple $(Q_i, T_i^{\text{prop}}, F_i^{\text{out}}, \vec{F}_i, \vec{P}r_i, \mathcal{Q}_i^{\mathcal{P}})$ where:

- 16 • Q_i is the maximum capacity of i ;
- 17 • T_i^{prop} is the time required to traverse i and reach the stop line;
- 18 • F_i^{out} represents the maximum traffic flow from i to the outside of the modeled network;
- 19 • \vec{F}_i and $\vec{P}r_i$ are vectors of size $|\mathcal{Q}|$ and their j -th entry (i.e., $F_{i,j}$ and $\text{Pr}_{i,j}$) represent the
 20 maximum flow from queue i to j and the turn probability from i to j ($\sum_{j \in \mathcal{Q}} \text{Pr}_{i,j} = 1$),
 21 respectively; and
- 22 • $\mathcal{Q}_i^{\mathcal{P}}$ denotes the set of traffic light phases controlling the outflow of queue i .

23 Differently than the CTM (9, 14), the QTM does not assume that $\Delta t_n = T_i^{\text{prop}}$ for all n , that
 24 is, the QTM can represent non-homogeneous time intervals (Figure 1(b)). The only requirement
 25 over Δt_n is that no traffic light maximum phase time is smaller than any Δt_n since phase changes
 26 occur only between time intervals; formally, $\Delta t_n \leq \min_{\ell \in \mathcal{L}, k \in \mathcal{P}_\ell} \Phi_{\ell,k}^{\max}$ for all $n \in \{1, \dots, N\}$.

27 Computing Traffic Flows with QTM

28 In this section, we present how to compute traffic flows using QTM and non-homogeneous time
 29 intervals Δt . We assume for the remainder of this section that a *valid* control plan for all traffic
 30 lights is fixed and given as parameter; formally, for all $\ell \in \mathcal{L}$, $k \in \mathcal{P}_\ell$, and interval $n \in \{1, \dots, N\}$,
 31 the binary variable $p_{\ell,k,n}$ is known a priori and indicates if phase k of light ℓ is active (i.e., $p_{\ell,k,n} =$
 32 1) or not on interval n .

33 We represent the problem of finding the maximal flow between capacity-constrained queues
 34 as a Linear Program (LP) over the following variables defined for all interval $n \in \{1, \dots, N\}$ and
 35 queues i and j :

- 36 • $q_{i,n} \in [0, Q_i]$: traffic volume waiting in the stop line of queue i at the beginning of
 1 interval n ;

- 2 • $f_{i,n}^{\text{in}} \in [0, I_{i,n}]$: inflow to the network via queue i during interval n ;
- 3 • $f_{i,n}^{\text{out}} \in [0, F_i^{\text{out}}]$: outflow from the network via queue i during interval n ; and
- 4 • $f_{i,j,n} \in [0, F_{i,j}]$: flow from queue i into queue j during interval n .

5 The maximum traffic flow from queue i to queue j is enforced by constraints (C1) and (C2).
 6 (C1) ensures that only the fraction $\text{Pr}_{i,j}$ of the total internal outflow of i goes to j , and (C2) forces
 7 the flow from i to j to be zero if all phases controlling i are inactive (i.e., $p_{\ell,k,n} = 0$ for all $k \in \mathcal{Q}_i^P$).
 8 If more than one phase $p_{\ell,k,n}$ is active, then (C2) is subsumed by the domain upper bound of $f_{i,j,n}$.

$$9 \quad f_{i,j,n} \leq \text{Pr}_{i,j} \sum_{k=1}^{|\mathcal{Q}|} f_{i,k,n} \quad (\text{C1})$$

$$10 \quad f_{i,j,n} \leq F_{i,j} \sum_{p_{\ell,k,n} \in \mathcal{Q}_i^P} p_{\ell,k,n} \quad (\text{C2})$$

12 To simplify the presentation of remainder of the LP, we define the helper variables $q_{i,n}^{\text{in}}$ (C3),
 13 $q_{i,n}^{\text{out}}$ (C4), and t_n (C5) to represent the volume of traffic to enter and leave queue i during interval n ,
 14 and the time elapsed since the beginning of the problem until the end of interval Δt_n , respectively.

$$15 \quad q_{i,n}^{\text{in}} = \Delta t_n (f_{i,n}^{\text{in}} + \sum_{j=1}^{|\mathcal{Q}|} f_{j,i,n}) \quad (\text{C3})$$

$$16 \quad q_{i,n}^{\text{out}} = \Delta t_n (f_{i,n}^{\text{out}} + \sum_{j=1}^{|\mathcal{Q}|} f_{i,j,n}) \quad (\text{C4})$$

$$17 \quad t_n = \sum_{x=1}^n \Delta t_x \quad (\text{C5})$$

19 In order to account for the misalignment of the different Δt and T_i^{prop} , we need to find the
 20 volume of traffic that entered queue i between two arbitrary points in time x and y ($x \in [0, T]$,
 21 $y \in [0, T]$, and $x < y$), i.e., x and y might not coincide with any t_n for $n \in \{1, \dots, N\}$. This
 22 volume of traffic, denoted as $V_i(x, y)$, is obtained by integrating $q_{i,n}^{\text{in}}$ over $[x, y]$ and is defined in (1)
 23 where m and w are the index of the time intervals s.t. $t_m \leq x < t_{m+1}$ and $t_w \leq y < t_{w+1}$. Because
 24 the QTM dynamics are *piecewise linear*, $q_{i,n}^{\text{in}}$ is a step function w.r.t. time and this integral reduces
 25 to the sum of $q_{i,n}^{\text{in}}$ over the intervals contained in $[x, y]$ and the appropriate fraction of $q_{i,m}^{\text{in}}$ and $q_{i,w}^{\text{in}}$
 26 representing the misaligned beginning and end of $[x, y]$.

$$27 \quad V_i(x, y) = (t_{m+1} - x) \frac{q_{i,m}^{\text{in}}}{\Delta t_m} + \left(\sum_{k=m+1}^{w-1} q_{i,k}^{\text{in}} \right) + (y - t_w) \frac{q_{i,w}^{\text{in}}}{\Delta t_w} \quad (1)$$

28 Using these helper variables, (C6) represents the flow conservation principle for queue i
 29 where $V_i(t_{n-1} - T_i^{\text{prop}}, t_n - T_i^{\text{prop}})$ is the volume of cars that reached the stop line during Δt_n .
 30 Since Δt and T_i^{prop} for all queues are known a priori, the indexes m and w used by V_i can be pre-
 1 computed in order to encode (1); moreover, (C6) represents a non-first order Markovian update



FIGURE 2 Cumulative arrival (blue) and departure (green) curves, and the resulting delay curve (red). The departure curve is maximized by the objective function (O1), which has the same effect as minimizing the area under the delay curve.

2 because the update considers the previous $w - m$ time steps. To ensure that the total volume of
 3 traffic traversing i (i.e., $V_i(t_n - T_i^{\text{prop}}, t_n)$) and waiting at the stop line does not exceed the capacity
 4 of the queue, we apply (C7).

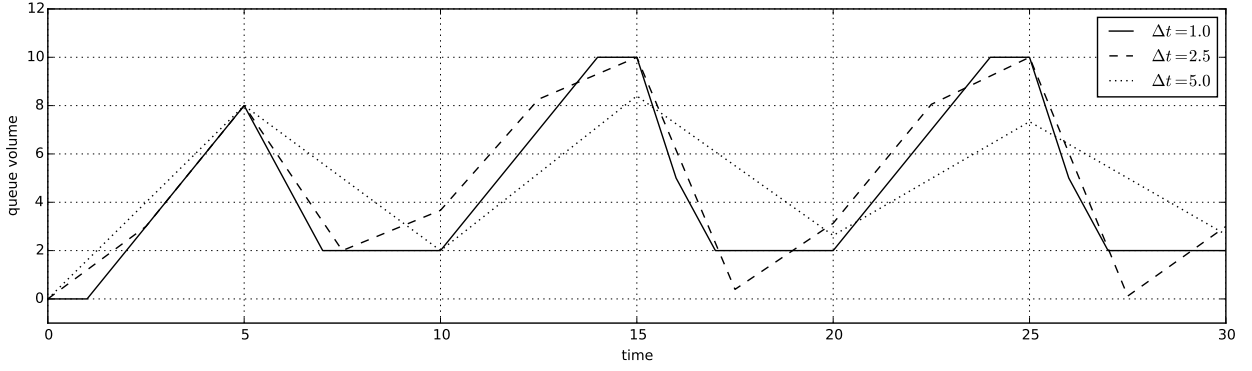
$$5 \quad q_{i,n} = q_{i,n-1} - q_{i,n-1}^{\text{out}} + V_i(t_{n-1} - T_i^{\text{prop}}, t_n - T_i^{\text{prop}}) \quad (\text{C6})$$

$$6 \quad V_i(t_n - T_i^{\text{prop}}, t_n) + q_{i,n} \leq Q_i \quad (\text{C7})$$

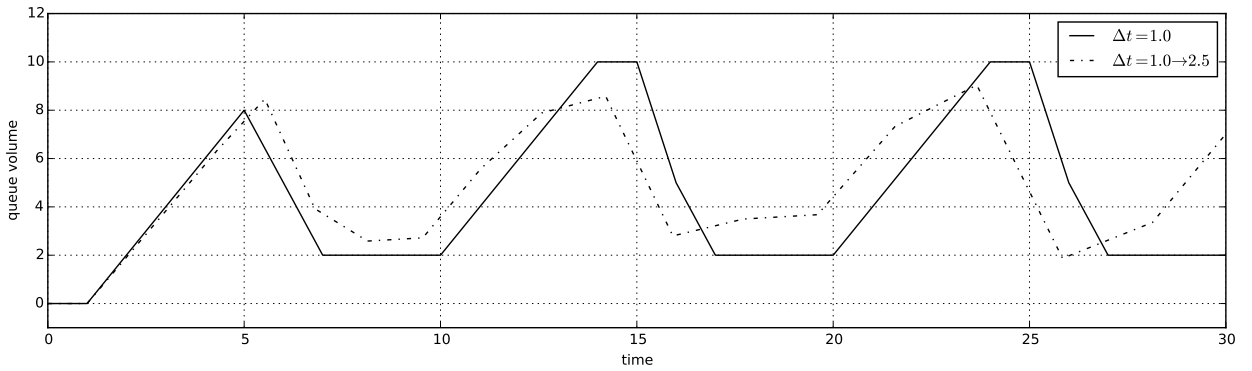
8 As with MILP formulations of CTM (e.g. Lin and Wang (9)), QTM is also susceptible to
 9 *withholding traffic*, i.e., the optimizer might prevent cars from moving from i to j even though
 10 the associated traffic phase is active and j is not full, e.g., this may reserve space for traffic from
 11 an alternate approach that allows the MILP to minimize delay in the long-term even though it
 12 leads to unintuitive traffic flow behavior. We address this well-known issue through our objective
 13 function (O1) by maximizing the total outflow $q_{i,n}^{\text{out}}$ (i.e., both internal and external outflow) of i
 14 plus the inflow $f_{i,n}^{\text{in}}$ from the outside of the network to i . This quantity is weighted by the remaining
 15 time until the end of the problem horizon T to force the optimizer to allow as much traffic volume
 16 as possible into the network and move traffic to the outside of the network as soon as possible.

$$17 \quad \max \sum_{n=1}^N \sum_{i=1}^{|Q|} (T - t_n + 1)(q_{i,n}^{\text{out}} + f_{i,n}^{\text{in}}) \quad (\text{O1})$$

18 The objective (O1) corresponds to minimizing delay in CTM models, e.g., (O1) is equiva-
 19 lent to the objective function (O3) in Lin and Wang (9) for their parameters $\alpha = \beta = 1$. Figure 2
 20 depicts this equivalence using the cumulative number of cars entering and leaving a network as a
 21 function of time. The delay experienced by the vehicles travelling through this network (red curve
 22 in Figure 2) equals the horizontal difference at each point between the cumulative departure and
 23 arrival curves (less the free flow travel time through the network). Maximizing $q_{i,n}^{\text{out}}$ weighted by
 24 $(T - t_n + 1)$ in (O1) is the same as forcing the departure curve to be as close as possible to the
 25 arrival curve as early as possible; therefore, the area between arrival and departure is minimized,
 1 which in turn minimizes the delay.



(a)



(b)

FIGURE 3 Approximations of a queue volume obtained using homogeneous $\Delta t = 1\text{s}$ using: (a) homogeneous $\Delta t = 2.5\text{s}$ and 5s ; and (b) non-homogeneous $\Delta t_n \approx 0.0956n + 0.9044$ for $n \in \{1, \dots, 17\}$. Here we see that (b) achieves accuracy in the near-term that somewhat degrades over the long-term, where accuracy will be less critical for receding horizon control.

To illustrate the representation tradeoff offered by non-homogeneous time intervals, we computed flows and queue volumes for a fixed signal control plan derived for homogeneous $\Delta t_n = 1\text{s}$ (ground truth) using different discretizations. Figure 3(a) shows the approximation of the ground truth using homogeneous $\Delta t = 2.5$ and $\Delta t = 5.0$, and Figure 3(b) using non-homogeneous time intervals that linearly increases from 1s to 2.5s , i.e., $\Delta t_n \approx 0.0956n + 0.9044$ for $n \in \{1, \dots, 17\}$. As Figure 3(a) shows, large time steps can be rough approximations of the ground truth. Non-homogeneous discretization (Figure 3(b)) exploits this fact to provide a good approximation in the initial time steps and progressively decrease precision for points far in the future.

11 TRAFFIC CONTROL WITH QTM ENCODED AS A MILP

In this section, we remove the assumption that a valid control plan for all traffic lights is given and extend the LP (O1, C1–C7) to an Mixed-Integer LP (MILP) that also computes the optimal control plan. Formally, for all $\ell \in \mathcal{L}$, $k \in \mathcal{P}_\ell$, and interval $n \in \{1, \dots, N\}$, the phase activation parameter $p_{\ell,k,n} \in \{0, 1\}$ becomes a free variable to be optimized. In order to obtain a valid control

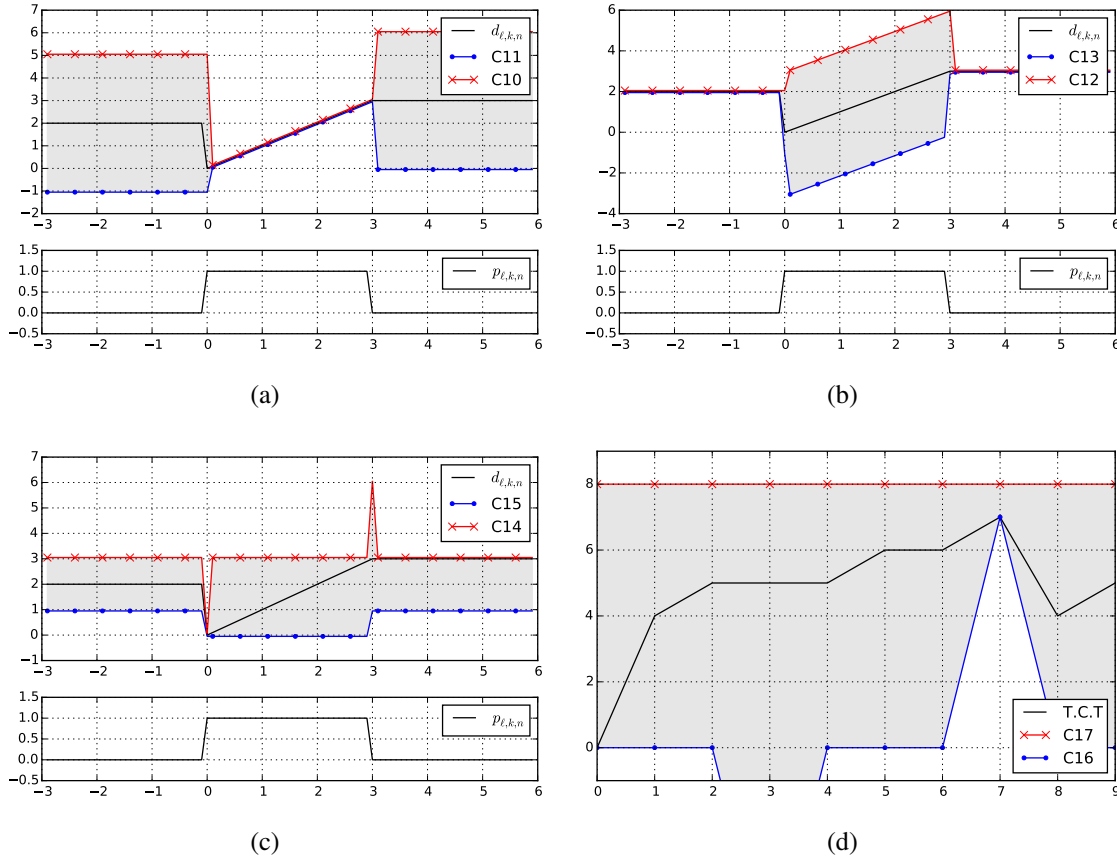


FIGURE 4 Visualization of constraints (C10–C17) for a traffic light ℓ as a function of time. (a–c) present, pairwise, the constraints (C10–C15) for phase k ($d_{\ell,k,n}$ as the black line) and the activation variable $p_{\ell,k,n}$ in the small plot. (d) presents the constraints for the cycle time of ℓ (C16 and C17), where T.C.T. is the total cycle time and is the left hand side of both constraints. For this example, $\Phi_{\ell,k}^{\min} = 1$, $\Phi_{\ell,k}^{\max} = 3$, $\Psi_{\ell}^{\min} = 7$, and $\Psi_{\ell}^{\max} = 8$.

2 plan, we enforce that one phase of traffic light ℓ is always active at any interval n (C8) and that
 3 phase changes happen sequentially (C9), i.e., if phase k was active during interval $n - 1$ and has
 4 become inactive in interval n , then phase $k + 1$ must be active in interval n . (C9) assumes that
 5 $k + 1$ equals 1 if $k = |\mathcal{P}_{\ell}|$.

$$6 \quad \sum_{k=1}^{|\mathcal{P}_{\ell}|} p_{\ell,k,n} = 1 \quad (C8)$$

$$7 \quad p_{\ell,k,n-1} \leq p_{\ell,k,n} + p_{\ell,k+1,n} \quad (C9)$$

9 Next, we enforce the minimum and maximum phase durations (i.e., $\Phi_{\ell,k}^{\min}$ and $\Phi_{\ell,k}^{\max}$) for
 10 each phase $k \in \mathcal{P}_{\ell}$ of traffic light ℓ . To encode these constraints, we use the helper variable
 11 $d_{\ell,k,n} \in [0, \Phi_{\ell,k}^{\max}]$, defined by constraints (C10–C14), that: (i) holds the elapsed time since the
 12 start of phase k when $p_{\ell,k,n}$ is active (C10,C11); (ii) is constant and holds the duration of the last
 1 phase until the next activation when $p_{\ell,k,n}$ is inactive (C12,C13); and (iii) is restarted when phase k

changes from inactive to active (C14). Notice that (C10–C14) employs the *big-M* method to turn the cases that should not be active into subsumed constraints based on the value of $p_{\ell,k,n}$. We use $\Phi_{\ell,k}^{\max}$ as our large constant since $d_{\ell,k,n} \leq \Phi_{\ell,k}^{\max}$ and $\Delta t_n \leq \Phi_{\ell,k}^{\max}$. Similarly, constraint (C15) ensures the minimum phase time of k and is not enforced while k is still active. Figures 4(a) to 4(c) present an example of how (C10–C15) work together as a function of the time n for $d_{\ell,k,n}$; the domain constraint $0 \leq d_{\ell,k,n} \leq \Phi_{\ell,k}^{\max}$ for all $n \in \{1, \dots, N\}$ is omitted for clarity.

$$d_{\ell,k,n} \leq d_{\ell,k,n-1} + \Delta t_{n-1} p_{\ell,k,n-1} + \Phi_{\ell,k}^{\max} (1 - p_{\ell,k,n-1}) \quad (\text{C10})$$

$$d_{\ell,k,n} \geq d_{\ell,k,n-1} + \Delta t_{n-1} p_{\ell,k,n-1} - \Phi_{\ell,k}^{\max} (1 - p_{\ell,k,n-1}) \quad (\text{C11})$$

$$d_{\ell,k,n} \leq d_{\ell,k,n-1} + \Phi_{\ell,k}^{\max} p_{\ell,k,n-1} \quad (\text{C12})$$

$$d_{\ell,k,n} \geq d_{\ell,k,n-1} - \Phi_{\ell,k}^{\max} p_{\ell,k,n} \quad (\text{C13})$$

$$d_{\ell,k,n} \leq \Phi_{\ell,k}^{\max} (1 - p_{\ell,k,n} + p_{\ell,k,n-1}) \quad (\text{C14})$$

$$d_{\ell,k,n} \geq \Phi_{\ell,k}^{\min} (1 - p_{\ell,k,n}) \quad (\text{C15})$$

Lastly, we constrain the sum of all the phase durations for light ℓ to be within the cycle time limits Ψ_{ℓ}^{\min} (C16) and Ψ_{ℓ}^{\max} (C17). In both (C16) and (C17), we use the duration of phase 1 of ℓ from the previous interval $n - 1$ instead of the current interval n because (C14) forces $d_{\ell,1,n}$ to be 0 at the beginning of each cycle; however, from the previous end of phase 1 until $n - 1$, $d_{\ell,1,n-1}$ holds the correct elapse time of phase 1. Additionally, (C16) is enforced right after the end of the each cycle, i.e., when its first phase is changed from inactive to active. The value (C16) and (C17) over time for a traffic light ℓ is illustrated in Figure 4(d).

$$d_{\ell,1,n-1} + \sum_{k=2}^{|\mathcal{P}_{\ell}|} d_{\ell,k,n} \geq \Psi_{\ell}^{\min} (p_{k,1,n} - p_{k,1,n-1}) \quad (\text{C16})$$

$$d_{\ell,1,n-1} + \sum_{k=2}^{|\mathcal{P}_{\ell}|} d_{\ell,k,n} \leq \Psi_{\ell}^{\max} \quad (\text{C17})$$

The MILP that encodes the problem of finding the optimal traffic control plan in a QTM network is defined by (O1, C1–C17).

EMPIRICAL EVALUATION

In this section we compare the solutions for traffic networks modeled as a QTM using homogeneous and non-homogeneous time intervals w.r.t. to two evaluation criteria: the quality of the solution and convergence to the optimal solution vs. the number of time steps. Specifically, we compare the quality of solutions based on the total travel time and we also consider the third quartile and maximum of the observed delay distribution. Our hypotheses are: (i) the quality of the non-homogeneous solutions is at least as good as the homogeneous ones when the number of time intervals N is fixed; and (ii) the non-homogeneous approach requires less time intervals (i.e., smaller N) than the homogeneous approach to converge to the optimal solution. In the remainder of this section, we present the traffic networks considered in the experiments, our methodology, and the results.



FIGURE 5 (a–c) Networks used to evaluate the QTM performance. (d) Demand profile of the queues marked as \diamond , \clubsuit , and \spadesuit for our experiments.

38 Networks

1 We consider three networks of increasing complexity (Figure 5): an avenue crossed by three side
2 streets; a 2-by-3 grid; and a 3-by-3 grid with a diagonal avenue. The queues receiving cars from
3 outside of the network are marked in Figure 5 and we refer to them as input queues. The maximum
4 queue capacity (Q_i) is 60 cars for non-input queues and infinity for input queues to prevent inter-
5 ruption of the input demand due to spill back from the stop line. The traversal time of each queue
6 i (T_i^{prop}) is set at 9s (a distance of 125m with a free flow speed of 50km/h). For each street, flows
7 are defined from the head of each queue i into the tail of the next queue j ; there is no turning traffic
8 ($\text{Pr}_{i,j} = 1$), and the maximum flow rate between queues, $F_{i,j}$, is set at 5 cars/s. All traffic lights
9 have two phases, north-south and east-west, and lights 2, 4 and 6 of network 3 have the additional
10 northeast-southwest phase to control the diagonal avenue. For networks 1 and 2, $\Phi_{\ell,k}^{\min}$ is 1s, $\Phi_{\ell,k}^{\max}$
11 is 3s, Ψ_{ℓ}^{\min} is 2s, and Ψ_{ℓ}^{\max} is 6s, for all traffic light ℓ and phase k . For network 3, $\Phi_{\ell,k}^{\min}$ is 1s and
12 $\Phi_{\ell,k}^{\max}$ is 6s for all ℓ and k ; and Ψ_{ℓ}^{\min} is 2s and Ψ_{ℓ}^{\max} is 12s for all lights ℓ except for lights 2, 4 and
13 6 (i.e., lights also used by the diagonal avenue) in which Ψ_{ℓ}^{\min} is 3s and Ψ_{ℓ}^{\max} is 18s.



FIGURE 6 Receding horizon control. In this example, the problem horizon T is 40s. The major frames for MILP optimization are discretized in 12 time intervals ($N = 12$) and they span 15s and 30s for homogeneous and non-homogeneous discretizations, respectively. The minor frames represent the prefix of the major frame MILP optimization that is executed. The horizon recedes by the minor frame duration after each execution.

14 Experimental Methodology

15 For each network, a constant background level traffic is injected in the network in the first 55s to
 16 allow the solver to settle on a stable policy. Then a spike in demand is introduced in the queues
 1 marked as ♠ (Figure 5) from time 55s to 70s to trigger a policy change. From time 70s to 85s,
 2 the demand is returned to the background level, and then reduced to zero for all input queues. We
 3 extend the problem horizon T until all cars have left the network. By clearing the network, we can
 4 easily measure the total travel time for all the traffic as the area between the cumulative arrival and
 5 departure curves measured at the boundaries of the network. The background level for the input
 6 queues are 1, 4 and 2 cars/s for queues marked as ♦, ♣ and ♠ (Figure 5(d)), respectively; and
 7 during the high demand period, the queues ♠ receive 4 cars/s.

8 For both homogeneous and non-homogeneous intervals, we use the MILP QTM formula-
 9 tion in a receding horizon manner: a control plan is computed for a pre-defined horizon (smaller
 10 than T) and only a prefix of this plan is executed before generating a new control plan. Figure 6
 11 depicts our receding horizon approach and we refer to the planning horizon as a major frame and
 12 its executable prefix as a minor frame. Notice that, while the plan for a minor frame is being
 13 executed, we can start computing the solution for the next major frame based on a forecast model.

14 To perform a fair comparison between the homogeneous and non-homogeneous discretiza-
 15 tions, we fix the size of all minor frames to 10s and force it to be discretized in homogeneous
 16 intervals of 0.25s. For the homogeneous experiments, Δt is kept at 0.25s throughout the major
 17 frame; therefore, given N , the major frame size equals $N/4$ seconds for the homogeneous ap-
 18 proach. For the non-homogeneous experiments, Δt linearly increases from 0.25s at the end of
 19 the minor frame to 1.0s at the end of the major frame; therefore, the major frame size used by
 20 the non-homogeneous approach is $10.375 + 0.625(N - 40)$ seconds for a given $N > 40$. Once
 21 we have generated a series of minor frames, we concatenate them into a single plan and compute
 22 the flow through the network using the QTM LP formulation with a fixed (homogeneous) Δt of
 23 0.25s. We also compare both receding horizon approaches against the optimal solution obtained
 24 by computing a single control plan for the entire control horizon (i.e., $[0, T]$) using a fixed Δt of
 25 0.25s.

For all our experiments, we used GurobiTM as the MILP solver with 12 threads on a 3.1GHz AMD OpteronTM 4334 processor with 12 cores. We limit the MIP gap accuracy to 0.1% and the time cutoff for solving a major frame to 3000s for the receding horizon approaches and unbounded in order to determine the optimal minimum travel time solution to which all other solutions are compared. All our results are averaged over five runs to account for Gurobi's stochastic strategies.

Results

Figures 7(a), 7(c) and 7(e) show, for each network, the increase in the total travel time w.r.t. the optimal solution as a function of N . As we hypothesized, the non-homogeneous discretization requires less time intervals (i.e., smaller N) to obtain a solution with the same total travel time. This is important because the size of the MILP, including the number of binary variables, scales linearly with N ; therefore, the non-homogeneous approach can scale up better than the homogeneous one (e.g., Figure 7(e)). Also, for homogeneous and non-homogeneous discretizations, finding the optimal solution of major frames with large N might require more time than our imposed 3000s time cutoff and, in this case, Gurobi returns a feasible control plan that is far from optimal. The effect in the total travel time of these poor solutions can be seen in Figure 7(e) for $N > 120$.

The distribution of the total delay observed by each car while traversing the network is shown in Figures 7(b), 7(d) and 7(f). Each group of box plots represents a different value of N : when the non-homogeneous Δt first converges; when the homogeneous Δt first converges; and the optimum solution itself. In all networks, the quality of the solution obtained using non-homogeneous Δt is better or equal than using homogeneous Δt for fixed N in both the total travel time and *fairness*, i.e., smaller third quartile and maximum delay.

To further illustrate the differences between homogeneous and non-homogeneous discretizations, Figure 8 shows the cumulative arrival and departure curves and the how delay evolves over time for q_1 of network 2 (Figure 5(b)). In Figure 8(a), the comparison is done when non-homogeneous Δt first converges (i.e., point I in Figure 7(c)) and for this value of N , the major frame size in seconds of the non-homogeneous approach is 19.125s longer than the homogeneous one. This allows the MILP solver to “see” 19s further in the future when using non-homogeneous discretization and find a coordinated signal policy along the avenue to dissipate the extra traffic that arrives at time 55s. The shorter major frame of the homogeneous discretization does not allow the solver to adapt this far in advance and its delay observed after 55s is much larger than the non-homogeneous one. Once the homogeneous Δt has converged (Figure 8(b)), it is also able to anticipate the increased demand and adapt well in advance and both approaches generate solutions close to optimum (Figure 8(c)).

CONCLUSION

In this paper, we showed how to formulate a novel queue transmission model (QTM) model of traffic flow with non-homogeneous time steps as a linear program. We then proceeded to allow the traffic signals to become discrete variables subject to a delay minimizing optimization objective and standard traffic signal constraints leading to a final MILP formulation of traffic signal control with non-homogeneous time steps. We experimented with this novel QTM-based MILP control in a range of traffic networks and demonstrated that the non-homogeneous MILP formulation achieved (i) substantially lower delay solutions, (ii) improved per-car delay distributions, and (iii) more optimal travel times over a longer horizon in comparison to the homogeneous MILP formulation with the same number of binary and continuous variables. Altogether, this work represents

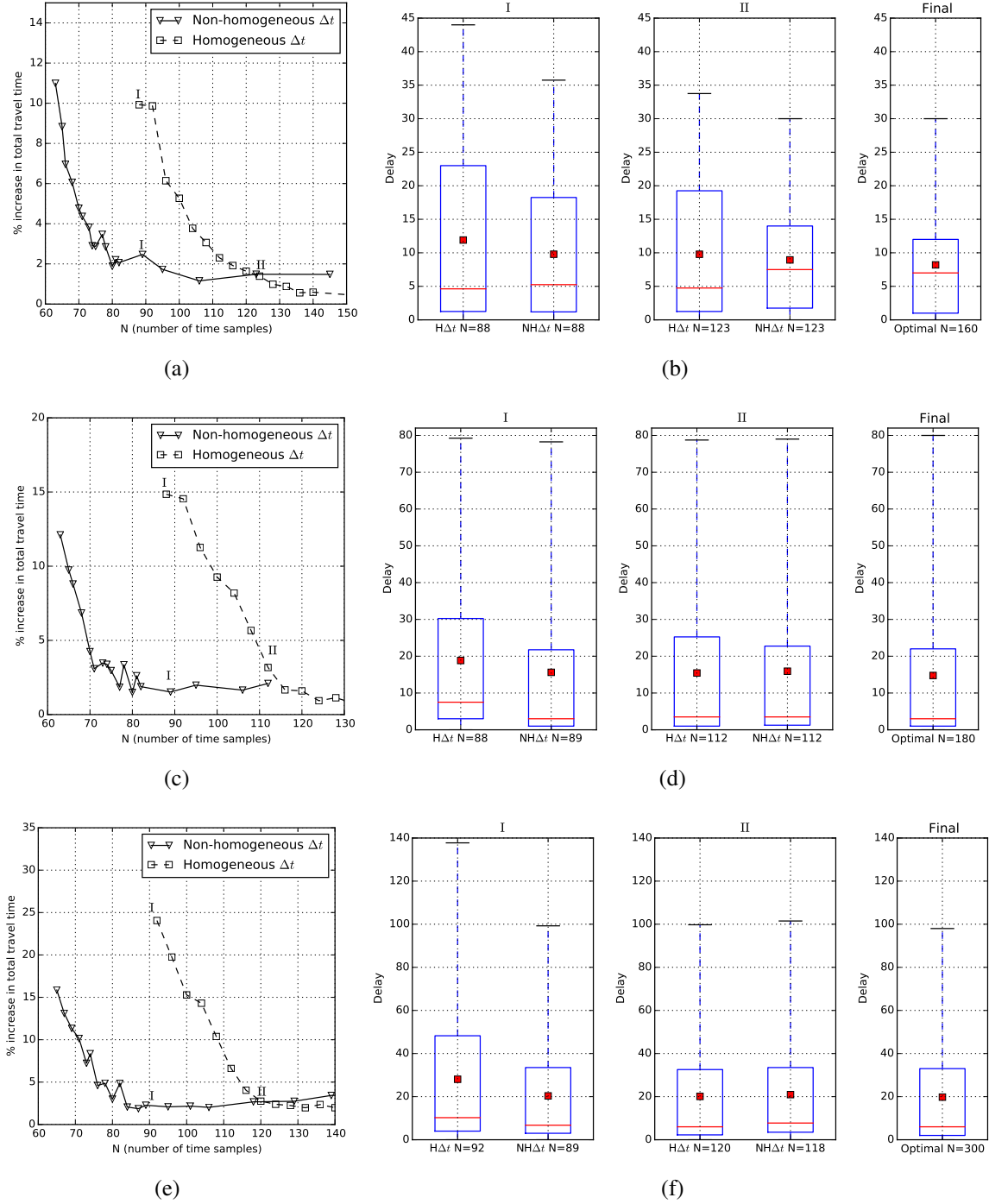


FIGURE 7 Increase in the total travel time w.r.t. the optimal solution as a function of N (a,c,e) and distribution of the total delay of each car for different values of N (b,d,f). For each row, the Roman numeral on top of the box plots corresponds to point the travel time plot marked with the same numeral. The mean of the total delay is presented as a red square in the box plots. Plots in the i -th row correspond to the results for the i -th network in Figure 5. Non-homogeneous (NH) achieves much better solutions at smaller N than Homogeneous (H).

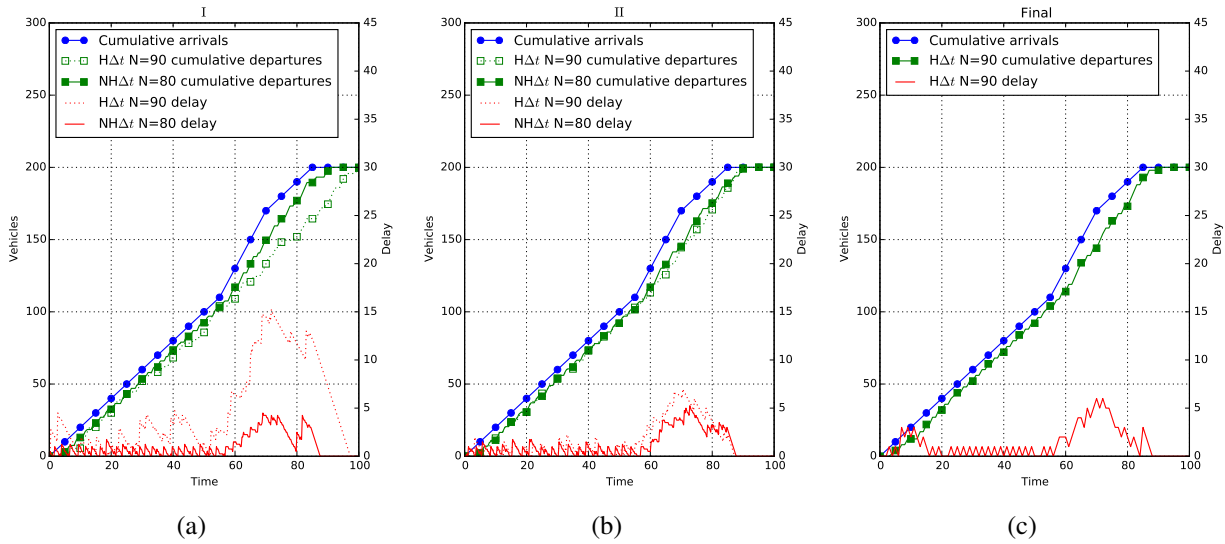


FIGURE 8 Cumulative arrival and departure curves and delay for queue 1 in the 2-by-3 network (Figure 5(b)). The labels on top of each plot match the labels in Figures 7(c) and 7(d). (c) presents the same curves for the optimal solution. Non-homogeneous (NH) provides near-optimal signal plans over a longer time horizon than Homogeneous (H) when the number of time intervals N is small.

a major step forward in the scalability of MILP-based jointly optimized traffic signal control via the use of a non-homogeneous time traffic models and thus helps pave the way for fully optimized joint urban traffic signal controllers as an improved successor technology to existing signal control methods.

ACKNOWLEDGMENT

This work is part of the Advanced Data Analytics in Transport programme, and supported by National ICT Australia (NICTA) and NSW Trade & Investment. NICTA is funded by the Australian Government through the Department of Communications and the Australian Research Council through the ICT Centre of Excellence Program. NICTA's role is to pursue potentially economically significant ICT related research for the Australian economy. NSW Trade & Investment is the business development agency for the State of New South Wales.

REFERENCES

- [1] Bazzan, A. L. C. and F. Klügl, *Introduction to Intelligent Systems in Traffic and Transportation*. Synthesis Lectures on Artificial Intelligence and Machine Learning, Morgan & Claypool Publishers, 2013.
- [2] El-Tantawy, S., B. Abdulhai, and H. Abdelgawad, Multiagent reinforcement learning for integrated network of adaptive traffic signal controllers (MARLIN-ATSC): methodology and large-scale application on downtown toronto. *Intelligent Transportation Systems, IEEE Transactions on*, Vol. 14, No. 3, 2013, pp. 1140–1150.
- [3] Sims, A. G. and K. W. Dobinson, SCAT—The Sydney co-ordinated adaptive traffic system:

- 36 Philosophy and benefits. *IEEE Transactions on Vehicular Technology*, Vol. 29, 1980.
- 37 [4] Hunt, P. B., D. I. Robertson, R. D. Bretherton, and R. I. Winton, *SCOOT—A traffic responsive*
38 *method of coordinating signals*. Transportation Road Research Lab, Crowthorne, U.K., 1981.
- 39 [5] Gartner, N., J. D. Little, and H. Gabbay, *Optimization of traffic signal settings in networks by*
1 *mixed-integer linear programming*. DTIC Document, 1974.
- 2 [6] Gartner, N. H. and C. Stamatiadis, Arterial-based control of traffic flow in urban grid net-
3 works. *Mathematical and computer modelling*, Vol. 35, No. 5, 2002, pp. 657–671.
- 4 [7] Lo, H. K., A novel traffic signal control formulation. *Transportation Research Part A: Policy*
5 *and Practice*, Vol. 33, No. 6, 1998, pp. 433–448.
- 6 [8] He, Q., K. L. Head, and J. Ding, PAMSCOD: Platoon-based Arterial Multi-modal Signal
7 Control with Online Data. *Procedia-Social and Behavioral Sciences*, Vol. 17, 2011, pp. 462–
8 489.
- 9 [9] Lin, W.-H. and C. Wang, An enhanced 0-1 mixed-integer LP formulation for traffic signal
10 control. *Intelligent Transportation Systems, IEEE Transactions on*, Vol. 5, No. 4, 2004, pp.
11 238–245.
- 12 [10] Han, K., T. L. Friesz, and T. Yao, A link-based mixed integer LP approach for adaptive traffic
13 signal control. *arXiv preprint arXiv:1211.4625*, 2012.
- 14 [11] Lo, H. K., E. Chang, and Y. C. Chan, Dynamic network traffic control. *Transportation Re-*
15 *search Part A: Policy and Practice*, Vol. 35, No. 8, 1999, pp. 721–744.
- 16 [12] He, Q., W.-H. Lin, H. Liu, and K. L. Head, Heuristic algorithms to solve 0–1 mixed integer
17 LP formulations for traffic signal control problems. In *Service Operations and Logistics and*
18 *Informatics (SOLI), 2010 IEEE International Conference on*, IEEE, 2010, pp. 118–124.
- 19 [13] Smith, S., G. Barlow, X.-F. Xie, and Z. Rubinstein, SURTRAC: Scalable Urban Traffic Con-
20 trol. In *Transportation Research Board 92nd Annual Meeting Compendium of Papers*, Trans-
21 portation Research Board, 2013.
- 22 [14] Daganzo, C. F., The cell transmission model: A dynamic representation of highway traffic
23 consistent with the hydrodynamic theory. *Transportation Research Part B: Methodological*,
24 Vol. 28, No. 4, 1994, pp. 269–287.
- 25 [15] Daganzo, C. F., The cell transmission model, part II: network traffic. *Transportation Research*
26 *Part B: Methodological*, Vol. 29, No. 2, 1995, pp. 79–93.
- 27 [16] Xiaojian, H., W. Wei, and H. Sheng, Urban traffic flow prediction with variable cell trans-
28 mission model. *Journal of Transportation Systems Engineering and Information Technology*,
29 Vol. 10, No. 4, 2010, pp. 73–78.
- 30 [17] Sumalee, A., R. Zhong, T. Pan, and W. Szeto, Stochastic cell transmission model (SCTM): A
31 stochastic dynamic traffic model for traffic state surveillance and assignment. *Transportation*
32 *Research Part B: Methodological*, Vol. 45, No. 3, 2011, pp. 507–533.

- 33 [18] Jabari, S. E. and H. X. Liu, A stochastic model of traffic flow: Theoretical foundations.
34 *Transportation Research Part B: Methodological*, Vol. 46, No. 1, 2012, pp. 156–174.
- 35 [19] Huang, K. C., *Traffic Simulation Model for Urban Networks: CTM-URBAN*. Ph.D. thesis,
36 Concordia University, 2011.
- 1 [20] Muralidharan, A., G. Dervisoglu, and R. Horowitz, Freeway traffic flow simulation using the
2 link node cell transmission model. In *American Control Conference, 2009. ACC'09.*, IEEE,
3 2009, pp. 2916–2921.
- 4 [21] Gomes, G. and R. Horowitz, Optimal freeway ramp metering using the asymmetric cell trans-
5 mission model. *Transportation Research Part C: Emerging Technologies*, Vol. 14, No. 4,
6 2006, pp. 244–262.
- 7 [22] Kim, Y., *Online traffic flow model applying dynamic flow-density relation*. Int. At. Energy
8 Agency, 2002.
- 9 [23] Lu, S., S. Dai, and X. Liu, A discrete traffic kinetic model—integrating the lagged cell trans-
10 mission and continuous traffic kinetic models. *Transportation Research Part C: Emerging*
11 *Technologies*, Vol. 19, No. 2, 2011, pp. 196–205.
- 415 [24] Alecsandru, C., A. Quddus, K. C. Huang, B. Rouhieh, A. R. Khan, and Q. Zeng, An as-
416 sessment of the cell-transmission traffic flow paradigm: Development and applications. In
417 *Transportation Research Board 90th Annual Meeting*, 2011, 11-1152.